

# Simultaneous Registration & Segmentation of Anatomical Structures from Brain MRI

Fei Wang<sup>1</sup> and Baba C. Vemuri<sup>1</sup>

Department of Computer & Information Sciences & Engr.,  
University of Florida, Gainesville, FL 32611  
{fewang, vemuri}@cise.ufl.edu \*

**Abstract.** *In this paper, we present a novel variational formulation of the registration assisted image segmentation problem which leads to solving a coupled set of nonlinear PDEs that are solved using efficient numerical schemes. Our work is a departure from earlier methods in that we have a unified variational principle wherein non-rigid registration and segmentation are simultaneously achieved; unlike previous methods of solution for this problem, our algorithm can accommodate for image pairs having very distinct intensity distributions. We present examples of performance of our algorithm on synthetic and real data sets along with quantitative accuracy estimates of the registration.*

## 1 Introduction

In Medical Imaging applications, segmentation can be a daunting task due to possibly large inhomogeneities in image intensities across an image e.g., in MR images. These inhomogeneities combined with volume averaging during the imaging and possible lack of precisely defined shape boundaries for certain anatomical structures complicates the segmentation problem immensely. One possible solution for such situations is atlas-based segmentation. The atlas once constructed can be used as a template and can be registered non-rigidly to the image being segmented (henceforth called a target image) thereby achieving the desired segmentation. Many of the methods that achieve atlas-based segmentation are based on a two stage process involving, (i) estimating the non-rigid deformation field between the atlas image and the target image and then, (ii) applying the estimated deformation field to the desired shape/atlas to achieve the segmentation of the corresponding structure/s in the target image. In this paper, we develop a novel technique that will simultaneously achieve the non-rigid registration and segmentation. There is a vast body of literature for the tasks of registration and segmentation independently however, methods that combine them into one algorithm are far and few in between. In the following, we will briefly review the few existing methods that attempt to achieve simultaneous registration and segmentation.

In one of the earliest attempts at joint registration & segmentation, Bansal et al., [1] developed a minmax entropy framework to rigidly register & segment portal and CT data sets. In [2], Yezzi et al., present a variational principle for

---

\* This research was in part funded by the NIH grants, RO1 NS046812 & NS42075. Authors thank Dr. C. M. Leonard of the UF Neuroscience Dept. for the hippocampal data sets.

achieving simultaneous registration and segmentation, however, the registration part is limited to rigid motions. A similar limitation applies to the technique presented by Noble et al., in [3]. A variational principle in a level-set based formulation was presented in Pargios et. al., [4], for segmentation and registration of cardiac MRI data. Their formulation was again limited to rigid motion and the experiments were limited to 2D images. In Fischl et al., [5], a Bayesian method is presented that simultaneously estimates a linear registration and the segmentation of a novel image. Note that linear registration does not involve non-rigid deformations. The case of joint registration and segmentation with non-rigid registration has not been addressed adequately in literature with the exception of the recent work reported in Soatto *et al.*, [6] and Vemuri *et al.*, [7]. However, these methods can only work with image pairs that are necessarily from the same modality or the intensity profiles are not too disparate.

In this paper, we present a unified variational principle that will simultaneously register the atlas shape (contour/surface) to the novel brain image and segment the desired shape (contour/surface) in the novel image. In this work, the atlas serves in the segmentation process as a prior and the registration of this prior to the novel brain scan will assist in segmenting it. Another key feature/strength of our proposed registration+segmentation scheme is that *it accommodates for image pairs having very distinct intensity distributions as in multimodality data sets*. More details on this are presented in section 2.

## 2 Registration+Segmentation Model

We now present our formulation of joint registration & segmentation model wherein it is assumed that the image to be segmented can be modeled by piecewise constant regions, as was done in [8]. This assumption simplifies our presentation but our model itself can be easily extended to the piecewise smooth regions case. Additionally, since we are only interested in segmenting a desired anatomical shape (e.g., the hippocampus, the corpus callosum, etc.), we will only be concerned with a binary segmentation i.e., two classes namely, voxels inside the desired shape and those that are outside it. These assumptions can be easily relaxed if necessary but at the cost of making the energy functional more complicated and hence computationally more challenging. Let  $I_1$  be the atlas image containing the atlas shape  $\bar{C}$ ,  $I_2$  the novel image that needs to be segmented and  $\mathbf{v}$  be the vector field, from  $I_2$  to  $I_1$  i.e., the transformation is centered in  $I_2$ , defining the non-rigid deformation between the two images. The variational principle describing our formulation of the registration assisted segmentation problem is given by:

$$\min E(\mathbf{v}, \tilde{C}) = Seg(I_2, \tilde{C}) + dist(\mathbf{v}(\bar{C}), \tilde{C}) + Reg(I_1, I_2, \mathbf{v}). \quad (1)$$

Where, the first term denotes the segmentation functional.  $\tilde{C}$  is the boundary contour (surface in 3D) of the desired anatomical shape in  $I_2$ . The second term measures the distance between the transformed atlas  $\mathbf{v}(\bar{C})$  and the current segmentation  $\tilde{C}$  in the novel brain image i.e., the target image and the third term denotes the non-rigid registration functional between the two images. Each of these functionals are given the following form:

$$Seg(I_2, \tilde{C}) = \int_{\Omega} (I_2 - u)^2 dx + \alpha \oint_{\tilde{C}} ds \quad (2)$$

Where,  $\Omega$  is the image domain and  $\alpha$  is a regularization parameter.  $u = u_i$  if  $x \in \tilde{C}_{in}$  and  $u = u_o$  if  $x \in \tilde{C}_{out}$ .  $\tilde{C}_{in}$  and  $\tilde{C}_{out}$  denote the regions inside and outside of the curve,  $\tilde{C}$  representing the desired shape boundaries in  $I_2$ .

For the non-rigid registration term in the energy function, we use the recently introduced information theoretic-based criteria [9] called the cross cumulative residual entropy (CCRE). In [9], CCRE was shown to outperform MI-based registration in the context of noise immunity and convergence range, motivating us to pick this criteria over the MI-based cost function. The new registration functional is defined by

$$Reg(I_1, I_2, \mathbf{v}) = - \left( \mathcal{C}(I_1(\mathbf{v}(\mathbf{x})), I_2(\mathbf{x})) + \mu \int_{\Omega} (\|\nabla \mathbf{v}(\mathbf{x})\|^2) \right) \quad (3)$$

where, cross-CRE  $\mathcal{C}(I_1(), I_2()) = \mathcal{E}(I_1) - E[\mathcal{E}(I_1/I_2)]$  and  $\mathcal{E}(\mathbf{I}_1) = - \int_{\mathcal{R}_+} P(|\mathbf{I}_1| > \lambda) \log P(|\mathbf{I}_1| > \lambda) d\lambda$  with  $\mathcal{R}_+ = (x \in \mathcal{R}; x \geq 0)$ .  $\mathbf{v}(\mathbf{x})$  is as before and  $\mu$  is the regularization parameter and  $\|\cdot\|$  denotes Frobenius norm. Using a B-spline representation of the non-rigid deformation, one need only compute this field at the control points of the B-splines and interpolate elsewhere, thus accruing computational advantages. Using this representation, we derived analytic expressions for the gradient of the energy with respect to the registration parameters. This in turn makes our optimization more robust and efficient.

In order for the registration and the segmentation terms to “talk” to each other, we need a connection term and that is given by

$$dist(\mathbf{v}(\tilde{C}), \tilde{C}) = \int_R \phi_{\mathbf{v}(\tilde{C})}(\mathbf{x}) d\mathbf{x} \quad (4)$$

Where,  $R$  is the region enclosed by  $\tilde{C}$ ,  $\phi_{\mathbf{v}(\tilde{C})}(\mathbf{x})$  is the embedding signed distance function of the contour  $\mathbf{v}(\tilde{C})$ , which can be used to measure the distance between  $\mathbf{v}(\tilde{C})$  and  $\tilde{C}$ . The level-set function  $\phi : \mathbb{R}^2 \rightarrow \mathbb{R}$  is chosen so that its zero level-set corresponds to the transformed template curve  $\mathbf{v}(\tilde{C})$ . Let  $E_{dist} := dist(\mathbf{v}(\tilde{C}), \tilde{C})$ , one can show that  $\frac{\partial E_{dist}}{\partial \tilde{C}} = \phi_{\mathbf{v}(\tilde{C})}(\tilde{C}) \mathbf{N}$  where  $\mathbf{N}$  is the normal to  $\tilde{C}$ . The corresponding curve evolution equation given by gradient descent is then

$$\frac{\partial \tilde{C}}{\partial t} = -\phi_{\mathbf{v}(\tilde{C})}(\tilde{C}) \mathbf{N} \quad (5)$$

Not only does the signed distance function representation make it easier for us to convert the curve evolution problem to the level-set framework (refer to section 3), it also facilitates the matching of the evolving curve  $\tilde{C}$  and the transformed template curve  $\mathbf{v}(\tilde{C})$ , and yet does not rely on a parametric specification of either  $\tilde{C}$  or the transformed template curve. Note that since  $dist(\mathbf{v}(\tilde{C}), \tilde{C})$  is a function of the unknown registration  $\mathbf{v}$  and the unknown segmentation  $\tilde{C}$ , it plays the crucial role of connecting the registration and the segmentation terms.

Combining these three functionals together, we get the following variational principle for the simultaneous registration+segmentation problem:

$$\begin{aligned} min E(\tilde{C}, \mathbf{v}, u_o, u_i) = & \int_{\Omega} (I_2 - u)^2 dx + \alpha_1 \oint_{\tilde{C}} ds + \alpha_2 dist(\mathbf{v}(\tilde{C}), \tilde{C}) \\ & - \alpha_3 \mathcal{C}(I_1(\mathbf{v}(\mathbf{x})), I_2(\mathbf{x})) + \alpha_4 \int_{\Omega} \|\nabla \mathbf{v}(\mathbf{x})\|^2 d\mathbf{x}. \end{aligned} \quad (6)$$

$\alpha_i$  are weights controlling the contribution of each term to the overall energy function and can be treated as unknown constants and either set empirically or estimated during the optimization process. This energy function is quite distinct from those used in methods existing in literature because it is achieving the Mumford-Shah type of segmentation in an active contour framework jointly with non-rigid registration and shape distance terms. We are now ready to discuss the level-set formulation of the energy function in the following section.

### 3 Level set formulation

We now present a level-set form of our formulation described earlier. For our model where the equation for the unknown curve  $\tilde{C}$  is coupled with the equations for  $\mathbf{v}(\mathbf{x})$ ,  $u_o$ ,  $u_i$ , it is convenient for us to use the level set approach as proposed in [8]. Taking the variation of  $E(\cdot)$  with respect to  $\tilde{C}$  and writing down the gradient descent leads to the following curve evolution equation:

$$\frac{\partial \tilde{C}}{\partial t} = - \left[ -(I_2 - u_i)^2 + (I_2 - u_o)^2 + \alpha_1 \kappa + \alpha_2 \phi_{\mathbf{v}(\tilde{C})}(\tilde{C}) \right] \mathbf{N} \quad (7)$$

Note that equation (5) is used in the derivation. Equation (7) in the level-set framework is given by:

$$\frac{\partial \phi}{\partial t} = \left[ -(I_2 - u_i)^2 + (I_2 - u_o)^2 + \alpha_1 \nabla \cdot \frac{\nabla \phi}{|\nabla \phi|} + \alpha_2 \phi_{\mathbf{v}(\tilde{C})}(\tilde{C}) \right] |\nabla \phi| \quad (8)$$

where  $u_i$  and  $u_o$  are the mean values inside and outside of the curve  $\tilde{C}$  in the image  $I_2$ .

As mentioned before, we use a B-spline basis to represent the displacement vector field  $\mathbf{v}(\mathbf{x}, \mu)$ , where  $\mu$  is the transformation parameters of the B-spline basis.

$$\frac{\partial E}{\partial \mu} = \alpha_2 \frac{\partial \int_R \phi_{\mathbf{v}(\tilde{C})}(\mathbf{x}) d\mathbf{x}}{\partial \mu} - \alpha_3 \frac{\partial \mathcal{C}(I_1(\mathbf{v}(\mathbf{x})), I_2(\mathbf{x}))}{\partial \mu} + \alpha_4 \frac{\partial \int_{\Omega} \|\nabla \mathbf{v}(\mathbf{x})\|^2 d\mathbf{x}}{\partial \mu} \quad (9)$$

The first term of equation(9) can be rewritten as follows:

$$\begin{aligned} \frac{\partial \int_R \phi_{\mathbf{v}(\tilde{C})}(\mathbf{x}) d\mathbf{x}}{\partial \mu} &= \int_R \frac{\partial \phi_{\mathbf{v}(\tilde{C})}(\mathbf{x})}{\partial \mu} d\mathbf{x} \\ &= \int_R \frac{\partial \phi_{\mathbf{v}(\tilde{C})}}{\partial v} \Big|_{v=\mathbf{v}(\mathbf{x}, \mu)} \cdot \frac{\partial \mathbf{v}(\mathbf{x}, \mu)}{\partial \mu} d\mathbf{x} \end{aligned} \quad (10)$$

where  $\frac{\partial \phi_{\mathbf{v}(\tilde{C})}}{\partial v}$  is the directional derivative in the direction of  $\mathbf{v}(\mathbf{x}, \mu)$ . The second term of equation(9) is more involved and tedious. We simply state the result here without the derivations for the sake of brevity,

$$\frac{\partial \mathcal{C}(I_2, I_1 \circ \mathbf{v}(x; \mu))}{\partial \mu} = \sum_{\lambda \in I_1} \sum_{k \in I_2} \log \frac{P(i > \lambda, k; \mu)}{p_{I_2}(k) P(i > \lambda; \mu)} \cdot \frac{\partial P(i > \lambda, k; \mu)}{\partial \mu} \quad (11)$$

where  $P(i > \lambda, k; \mu)$  and  $P(i > \lambda; \mu)$  are the joint and marginal cumulative residual distributions respectively.  $p_{I_2}(k)$  is the density function of image  $I_2$ . The last term of equation(9) leads to,

$$\frac{\partial \int_{\Omega} \|\nabla \mathbf{v}(\mathbf{x})\|^2 d\mathbf{x}}{\partial \mu} = 2 \int_{\Omega} \nabla \mathbf{v} \cdot \frac{\partial \mathbf{v}}{\partial \mu} d\mathbf{x} \quad (12)$$

where both the matrices  $\nabla \mathbf{v}$  and  $\frac{\partial \mathbf{v}}{\partial \mu}$  are vectorized before the dot product is computed.

Substituting equations (10), (11) and (12) respectively back into the equation (9), we get the analytical gradient of our energy function with respect to the B-spline transformation parameters  $\mu$ . We then solve for the stationary point of this nonlinear equation numerically using a quasi-Newton method.

### Algorithm Summary

Given atlas image  $I_1$  and the unknown subject’s brain scan  $I_2$ , we want the segmentation result  $\tilde{C}$  in  $I_2$ . Initialize  $\tilde{C}$  in  $I_2$  to be  $\bar{C}$ , set initial transformation parameters  $\mu_0$  to be zero.

1. Optimize  $\mu_i$  using equation (9) with Quasi-Newton method for one step. Update the deformation field  $\mathbf{v}(x; \mu_i)$ .
2. Evolve  $\phi$  in  $I_2$  using equation (8) for one step, update  $\bar{C}_i$  as the zero level-set of  $\phi$ .
3. Stop the registration process if the difference in consecutive iterates is less than  $\epsilon = 0.01$ , a pre-chosen tolerance, else go to **Step 1**.

## 4 Implementation Results

In this section, we present several examples results from an application of our algorithm. The results are presented for synthetic as well as real data. The first three experiments were performed in 2D, while the fourth one was performed in 3D. Note that the image pairs used in all these experiments have significantly different intensity profiles, which is unlike any of the previous methods, reported in literature, used for joint registration and segmentation. The synthetic data example contains a pair of MR T1 and T2 weighted images which are from the MNI brainweb site [10]. They were originally aligned with each other. We use the MR T1 image as the source image and the target image was generated from the MR T2 image by applying a known non-rigid transformation that was procedurally generated. In this case, we present the error in the estimated non-rigid deformation field, using our algorithm, as an indicator of the accuracy of estimated deformations.

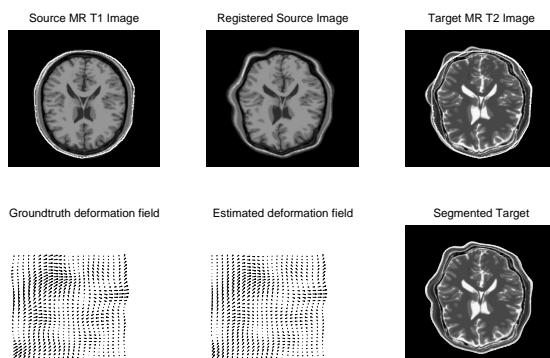


**Fig. 1.** Results of application of our algorithm to synthetic data (see text for details).

Figure 1 depicts the results obtained for this image pair. With the MR T1 image as the source image, the target was obtained by applying a synthetically

generated non-rigid deformation field to the MR T2 image. Notice the significant difference between the intensity profiles of the source and target images. Figure 1 is organized as follows, from left to right: the first row depicts the source image with the atlas-segmentation superposed in white, the registered source image which is obtained using our algorithm followed by the target image with the unregistered atlas-segmentation superposed to depict the amount of mis-alignment; second row depicts ground truth deformation field which we used to generate the target image from the MR T2 image, followed by the estimated non-rigid deformation field and finally the segmented target. As evident, the registration+segmentation are quite accurate from a visual inspection point of view. As a measure of accuracy of our method, we estimated the average,  $\mu$ , and the standard deviation,  $\sigma$ , of the error in the estimated non-rigid deformation field. The error was estimated as the angle between the ground truth and estimated displacement vectors. *The average and standard deviation are 1.5139 and 4.3211 (in degrees) respectively, which is quite accurate.*

Table 1 depicts statistics of the error in estimated non-rigid deformation when compared to the ground truth. For the mean ground truth deformation (magnitude of the displacement vector) in Column-1 of each row, 5 distinct deformation fields with this mean are generated and applied to the target image of the given source-target pair to synthesize 5 pairs of distinct data sets. These pairs (one at a time) are input to our algorithm and the mean ( $\mu$ ) of the mean deformation error (MDE) is computed over the five pairs and reported in Column-2 of the table. MDE is defined as  $d_m = \frac{1}{\text{card}(R)} \sum_{x_i \in R} \|\mathbf{v}_0(x_i) - \mathbf{v}(x_i)\|$ , where  $\mathbf{v}_0(x_i)$  is the ground truth and estimated displacements respectively at voxel  $x_i$ .  $\|\cdot\|$  denotes the Euclidean norm, and  $R$  is the volume of the region of interest. Column-3 depicts the standard deviation of the MDE for the five pairs of data in each row. As evident, the mean and the standard deviation of the error are reasonably small indicating the accuracy of our joint registration + segmentation algorithm. *Note that this testing was done on a total of 20 image pairs (=40) as there are 5 pairs of images per row.*

$\mu_g$	$\mu$ of MDE	$\sigma$ of MDE
2.4	0.5822	0.0464
3.3	0.6344	0.0923
4.5	0.7629	0.0253
5.5	0.7812	0.0714

**Table 1.** Statistics of the error in estimated non-rigid deformation.

For the first real data experiment, we selected two image slices from two different modalities of brain scans. The two slices depict considerable changes in shape of the ventricles, the region of interest in the data sets. One of the two slices was arbitrarily selected as the source and segmentation of the ventricle in the source was achieved using an active contour model. The goal was then to automatically find the ventricle in the target image using our algorithm given the input data along with the segmented ventricles in the source image. Figure 2 is organized as follows, from left to right: the first row depicts the source image with the atlas-segmentation superposed in black followed by the target image with the unregistered atlas-segmentation superposed to depict the amount

of mis-alignment; second row depicts the estimated non-rigid vector field and finally the segmented target. As evident from figures 2, the accuracy of the achieved registration+segmentation visually very good. Note that the non-rigid deformation between the two images in these two examples is quite large and our method was able to simultaneously register and segment the target data sets quite accurately.

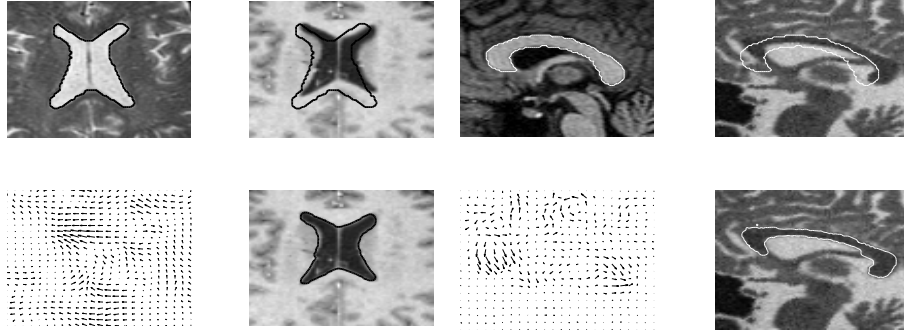


**Fig. 2.** Results of application of our algorithm to a pair of slices from human brain MRIs (see text for details).

**Fig. 3.** Corpus Callosum segmentation on a pair of corresponding slices from distinct subjects.

The second real data example is obtained from two brain MRIs of different subjects and modalities, the segmentation of the cerebellum in the source image is given. We selected two “corresponding” slices from these volume data sets to conduct the experiment. Note that even though the number of slices for the two data sets are the same, the slices may not correspond to each other from an anatomical point of view. However, for the purposes of illustration of our algorithm, this is not very critical. We use the corresponding slice of the 3D segmentation of the source as our atlas-segmentation. The results of an application of our algorithm are organized as before in figure 3. Once again, as evident, the visual quality of the segmentation and registration are very high.

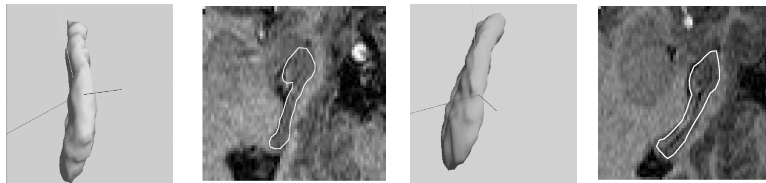


**Fig. 4.** Hippocampal segmentation using our algorithm on a pair of brain scans from distinct subjects. (see text for details)

Finally we present a 3D real data experiment. In this experiment, the input is a pair of 3D brain scans with the segmentation of the hippocampus in one of the two images (labeled the atlas image) being obtained using the well known PCA on the several training data sets. Each data set contains 19 slices of size 256x256. The goal was then to automatically find the hippocampus in the target image given the input. Figure 4 depicts the results obtained for this image pair. From

left to right, the first image shows the given (atlas) hippocampus surface followed by one cross-section of this surface overlaid on the source image slice; the third image shows the segmented hippocampus surface from the target image using our algorithm and finally the cross-section of the segmented surface overlaid on the target image slice. To validate the accuracy of the segmentation result, we randomly sampled 120 points from the segmented surface and computed the average distance from these points to the ground truth hand segmented hippocampal surface in the target image. The hand segmentation was performed by an expert neuroanatomist. The average and standard deviation of the error in the aforementioned distance in estimated hippocampal shape are 0.8190 and 0.5121(in voxels) respectively, which is very accurate.

## 5 Conclusions

In this paper, we presented a novel variational formulation of the joint (non-rigid) registration and segmentation problem which requires the solution to a coupled set of nonlinear PDEs that are solved using efficient numerical schemes. Our work is a departure from earlier methods in that we have a *unified variational principle* wherein non-rigid registration and segmentation are simultaneously achieved, our algorithm can also accommodate for image pair having distinct intensity distributions. We presented several examples (twenty) on synthetic and (three) real data sets along with quantitative accuracy estimates of the registration in the synthetic data case. More extensive experimentation under different amounts of noise and varying degrees of non-rigidity needs to be performed prior to drawing conclusions on the accuracy of the proposed model. This will be the focus of our future efforts.

## References

1. Bansal, R., Staib, L., Chen, Z., Rangarajan, A., Knisely, J., Nath, R., Duncan, J.: Entropy-based, multiple-portal-to-3dct registration for prostate radiotherapy using iteratively estimated segmentation. In: MICCAI. (1999) 567–578
2. Yezzi, A., Zollei, L., Kapur, T.: A variational framework for joint segmentation and registration. In: IEEE CVPR - MMBIA. (2001) 388–400
3. Wyatt, P., Noble, J.: Mrf-map joint segmentation and registration. In: MICCAI. (2002) 580–587
4. Paragios, N., Rousson, M., Ramesh, V.: Knowledge-based registration & segmentation of the left ventricle: A level set approach. In: WACV. (2002) 37–42
5. Fischl, B., Salat, D., Buena, E., et.al., M.A.: Whole brain sementation: Automated labeling of the neuroanatomical structures in the human brain. In: Neuron. Volume 33. (2002) 341–355
6. Soatto, S., Yezzi, A.J.: Deformation: Deforming motion, shape average and the joint registration and segmentation of images. In: ECCV. (2002) 32–57
7. Vemuri, B.C., Chen, Y., Wang, Z.: Registration assisted image smoothing and segmentation. In: ECCV. (2002) 546–559
8. Chan, T., Vesse, L.: An active contour model without edges. In: Intl. Conf. on Scale-space Theories in Computer Vision. (1999) 266–277
9. Wang, F., Vemuri, B.C., Rao, M., Chen, Y.: A new & robust information theoretic measure and its application to image alignment. In: IPMI. (2003) 388–400
10. : Mcconnell brain imaging centre brain database. <http://www.bic.mni.mcgill.ca/brainweb/> (1997)